FLUIDIC TUNING OF A FOUR-ARM SPIRAL-BASED FREQUENCY SELECTIVE SURFACE

A Thesis

by

ELIZABETH CHRISTINE WELLS

Submitted to the Office of Graduate Studies of
Texas A&M University
in partial fulfillment of the requirements for the degree of

MASTER OF SCIENCE

May 2011

Major Subject: Electrical Engineering

FLUIDIC TUNING OF A FOUR-ARM SPIRAL-BASED FREQUENCY SELECTIVE SURFACE

A Thesis

by

ELIZABETH CHRISTINE WELLS

Submitted to the Office of Graduate Studies of
Texas A&M University
in partial fulfillment of the requirements for the degree of

MASTER OF SCIENCE

Approved by:

Chair of Committee,	Gregory Huff
Committee Members,	Arum Han
	Jean-Francois Chamberland
	Krzysztof Michalski
Head of Department,	Scott Miller

May 2011

Major Subject: Electrical Engineering

ABSTRACT

Fluidic Tuning of a Four-Arm Spiral-Based Frequency Selective Surface. (May 2011)

Elizabeth Christine Wells, B.S., Texas A&M University

Chair of Advisory Committee: Dr. Gregory Huff

Frequency selective surfaces (FSSs) provide a variety of spatial filtering functions, such as band-pass or band-stop properties in a radome or other multilayer structure. This filtering is typically achieved through closely-spaced periodic arrangements of metallic shapes on top of a dielectric substrate (or within a stack of dielectric materials). In most cases, the unit cell size, its shape, the substrate parameters, and the inter-element spacing collectively impact the response of the FSS. Expanding this design space to include reconfigurable FSSs provides opportunities for applications requiring frequency agility and/or other properties. Tuning can also enable operation over a potentially wider range of frequencies and can in some cases be used as a loading mechanism or quasi-ground plane. Many technologies have been considered for this type of agility (RF MEMS, PIN diodes, etc.). This includes the recent use of microfluidics and dispersions of nanoparticles, or fluids with controllable dielectrics, which have entered the design space of numerous other EM applications including stub-tuners, antennas, and filters. In this work they provide a material based approach to reconfiguring an FSS.

An FSS based on a four-arm spiral with tunable band-stop characteristics is presented in this work. A thin colloidal dispersion above each element provides this tuning capability. The radial expansion and contraction of this dispersion, as well as the variable permittivity of the dispersion, are used to load each element individually. This design incorporates thin fluidic channels within a PDMS layer below the substrate leading to individual unit cells that provide a closed pressure-driven subsystem that contains the dispersion. With the capability to individually control each cell, groups of cells can be locally altered (individually or in groups) to create gratings and other electromagnetically agile features across the surface or within the volume of a radome or other covering. Simulations and measurements of an S-band tunable design using colloidal Barium Strontium Titanate dispersed Silicone oil are provided to demonstrate the capability to adjust the stop-band characteristics of the FSS across the S-band.

ACKNOWLEDGEMENTS

I would like to thank my committee chair, Dr. Huff, for his guidance and support throughout the course of this research. I would also like to thank Dr. Han for allowing me to use his lab. Thank you to my other committee members, Dr. Chamberland and Dr. Michalski for their participation on my committee.

Thanks also go to my friends and colleagues and the department faculty and staff for making my time at Texas A&M University a great experience. I also want to extend my gratitude to the U.S. National Science foundation and the U.S. Air Force Office of Scientific Research for their support.

Finally, thanks to my mother and father for their encouragement and to my husband for his patience and love.

NOMENCLATURE

FSS	Frequency Selective Surface
RF	Radio Frequency
BSTO	Barium Strontium Titanate Oxide
Si	Silicone
PDMS	Polydimethylsiloxane
φ	Volume Fraction
ε	Permittivity
dB	Decibels
GHz	Gigahertz
Freq	Frequency
S12	Reverse Voltage Gain, Transmission
IL	Insertion Loss

TABLE OF CONTENTS

CHAPTER Page

LIST OF FIGURES

FIGURE Page

FIGURE Page

FIGURE Page

LIST OF TABLES

CHAPTER I

INTRODUCTION

Frequency selective surfaces (FSSs) can provide many different filtering functions (i.e. band-pass, band-stop). This filtering is achieved through periodic arrangements of metallic shapes on top of a dielectric substrate. Unit cell size and shape, substrate parameters, and inter-element spacing affect the system response. The use of multiple layers [1]-[4] expands the design space and filtering possibilities.

Recent work [5-7] has focused on expanding this design space to include reconfigurable FSSs suitable for applications requiring frequency agility. Tuning enables operation over a potentially wider range of frequencies. In addition, tuning mechanisms can compensate for fabrication errors and/or discrepancies regarding substrates' characteristics. The integration of nonlinear devices such as varactors and electromechanical devices (e.g., RF MEMS) has been used in [5]-[7] to adjust the apparent size of the dielectric substrate below the FSS. Resonant frequency can be decreased or increased by increasing or decreasing the substrate dimensions respectively.

Recently, micro-fluidics and the use of dispersions (fluidic dielectrics) have entered the design space of numerous EM applications including stub-tuners [8], antennas [9], and filters [10]. Similarly, micro-fluidics provides a material-based approach to reconfiguring an FSS.

This work presents a tunable spiral-based FSS which achieves tuning through

---

This thesis follows the style of *IEEE Transactions on Microwave Theory and Techniques*.

varying the radius and relative permittivity of a cylindrical dielectric dispersion above each unit cell. Tuning an FSS across the S-band (2.6 – 4.0 GHz) represents the objective of this work. Static tests provide a proof of concept to the tuning capability. A fluidic network is constructed with channels leading to individual unit cells that provide the microfluidic colloidal dispersions. The capability to individually control each cell allows localization of groups of cells to create "openings" within the surface.

The design and operation of the FSS is presented in Chapter II. In Chapter III, the materials that are used in tuning the FSS are discussed. The experimental results are shown in Chapters IV-VI. Finally, concluding remarks and a design summary are presented in Chapter VII.

CHAPTER II

FOUR-ARM SPIRAL FREQUENCY SELECTIVE SURFACE

Design

A frequency selective surface uses a combination of inductance and capacitance on top of a dielectric to create a filter-like structure. Fig. 2.1 shows a diagram of a single four arm spiral in the unit cell prior to the addition of a colloidal dispersion. The spiral is on a 20 mil sheet of Duroid 5880.

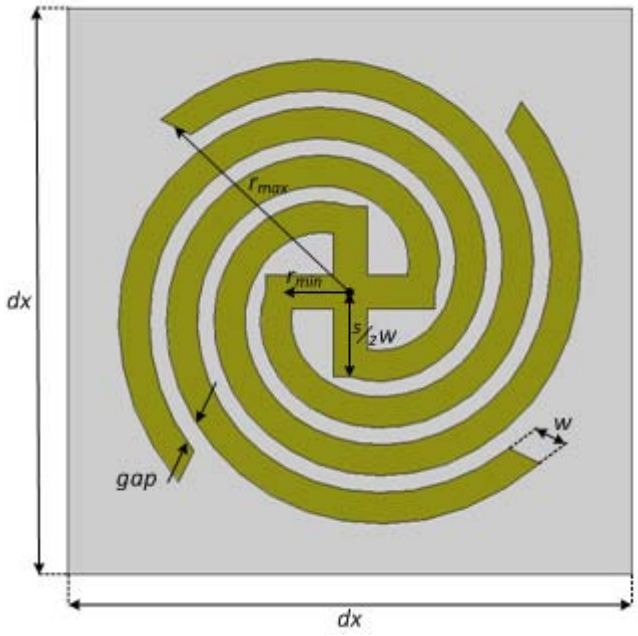

Fig. 2.1. Four-Arm FSS unit cell diagram.

The unit cells create a band-stop filter when arranged periodically. The spiraling of the arms allows an electrically resonant element to fit within a smaller unit cell. The inductance of the arms and the combined capacitance of the gaps between the arms and

the adjacent spirals create a band-stop filter. A circuit model of the spiral is shown in Fig. 2.2. The terms L_{spiral} and C_{spiral} represent the inductance and capacitance of the four-arm spiral. The term C_m represents the mutual capacitance between unit cells.

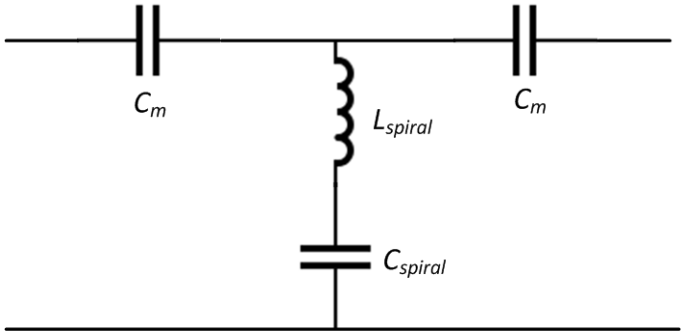

Fig. 2.2. Circuit diagram of four-arm spiral.

Equation 3.1 shows the relationship between resonant frequency and total inductance and capacitance of a filter. The parameters, L_{spiral}, C_{spiral}, and C_m, are all functions of the spiral geometry. Equations 3.2-3.3 show the relationship between the filter geometry and the inductances and capacitances. Tuning of L_{spiral} and C_{spiral} can be used to reconfigure the stop-band.

$$f_0 = \frac{1}{2\pi\sqrt{LC}} \tag{3.1}$$

$$L_{spiral} = f(r_{\min}, r_{\max}, w) \tag{3.2}$$

$$C_{spiral} = f(gap, \varepsilon_r, w) \tag{3.3}$$

Simulations

The FSS is simulated in HFSS as an infinite array. Master and Slave boundaries along with Floquet Ports create an infinite mirror boundary as seen in [11]. Fig. 2.3 shows the boundaries used in HFSS. The result of the simulation is shown in Fig. 2.4. The resonant frequency, f_0 is 3.872 GHz. Table 2.1 displays the parameters of the spiral in terms of the resonant wavelength.

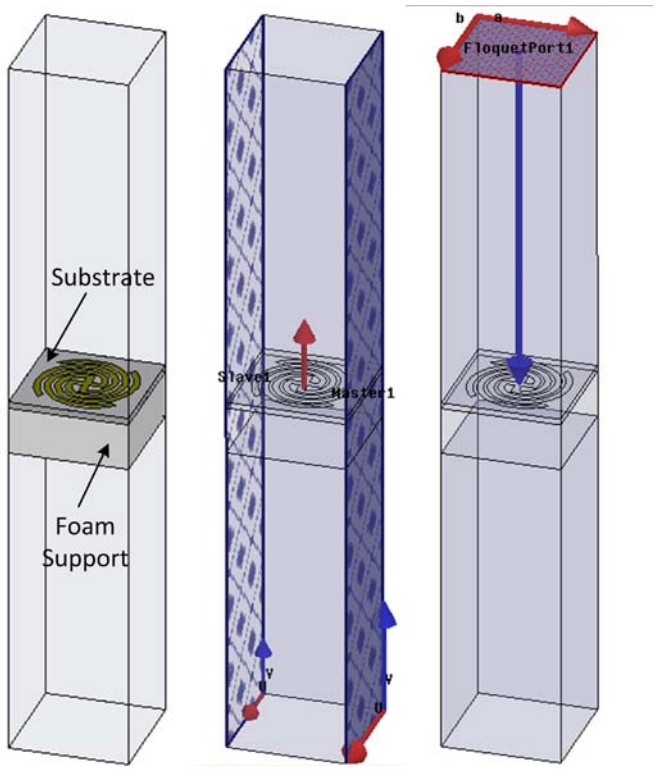

Fig. 2.3. HFSS simulated infinite array with Master-Slave boundaries.

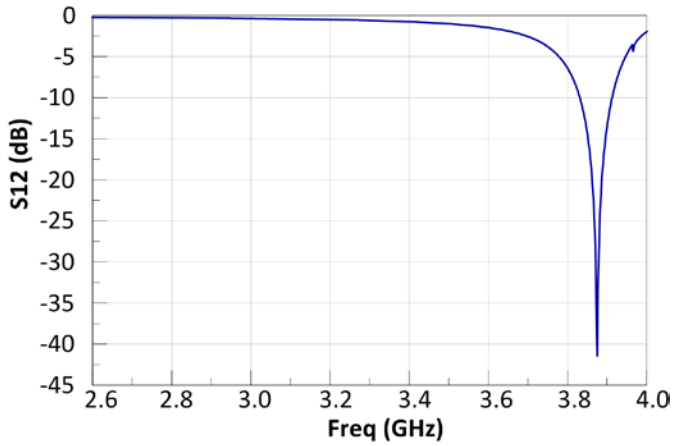

Fig. 2.4. Simulated S12 plot for simulated infinite FSS.

Table 2.1
FSS Unit Cell Parameters

dx	r_{max}	r_{min}	w	gap	N	Δr
$0.129\lambda_0$	$0.055\lambda_0$	$0.015\lambda_0$	$0.008\lambda_0$	$0.003\lambda_0$	0.880	$0.044\lambda_0$

Having four arms, as opposed to having two, creates greater rotational symmetry to reduce dependence on the incident wave's polarization. The four-arm spiral provides for TE and TM functionality. Figs. 2.5-2.6 compare TE and TM polarization for the two-arm and four-arm spiral. There is no difference in the transmission of the wave for TE versus TM for the four-arm spiral. However, the two-arm spiral is sensitive to TE and TM polarization because it is only symmetrical along one axis.

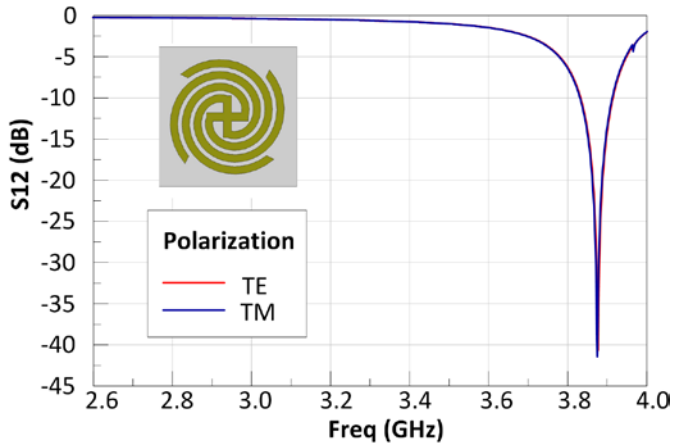

Fig. 2.5. Simulated S12 for TE and TM polarization for a four-arm spiral FSS.

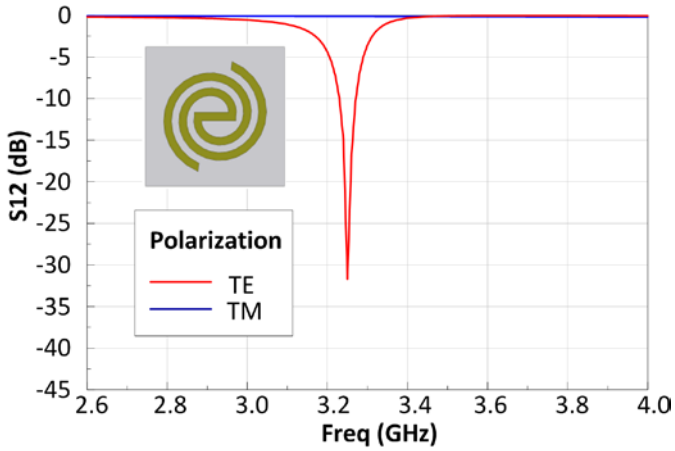

Fig. 2.6. Simulated S12 for TE and TM polarization for a two-arm spiral FSS.

The spiral also supports a wide angle of incidence away from broadside. Multiple angles of incidence were tested on the FSS using HFSS. The results are shown in Fig. 2.7. There is little difference in the operation of the filter based on angle of incidence.

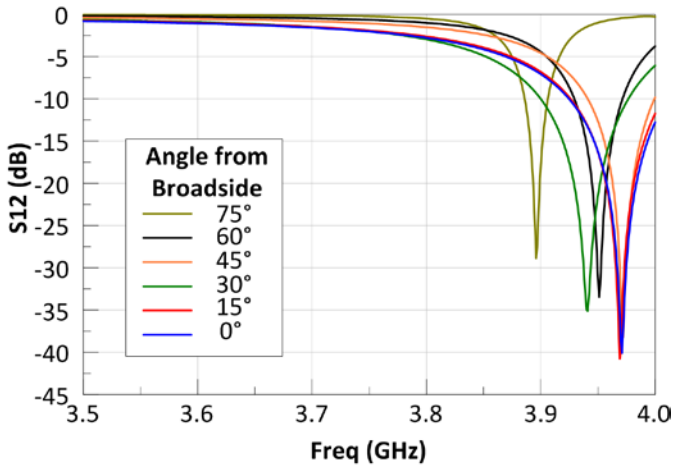

Fig. 2.7. Simulated S12 plot for various angles of incidence.

Dispersion Effect

The addition of a dielectric cylinder increases capacitance between the arms. Expanding this cylinder exposes more of the spiral to this effect and lowers the resonant frequency further. Increasing the permittivity of the cylinder also results in lowering the resonant frequency further. Fig. 2.8 shows the unit cell with the cylindrical dispersion.

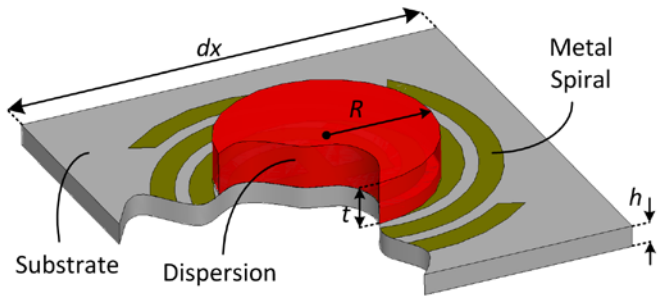

Fig. 2.8. Four-arm FSS unit cell diagram with dispersion.

A modified circuit of the FSS is shown in Fig. 2.9. A variable capacitor represents the tunable capacitance of the individual spiral elements.

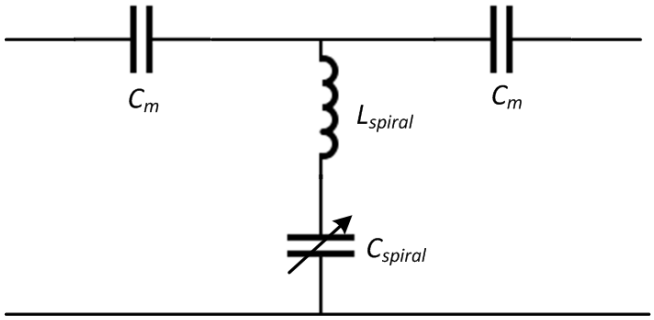

Fig. 2.9. Circuit diagram of four-arm spiral with variable capacitor representing tuning capability of spiral capacitance.

The tuning is simulated in HFSS by placing a cylinder above the spiral and running a parametric sweep on its radius and relative permittivity. Figs. 2.10-2.11 show the results of these sweeps. A radius of 2 mm to 4.5 mm is chosen because these are the range of radii that will be used in measurements. Also, a relative permittivity range of 1 to 11 is chosen because this is maximum range that can be achieved with the available materials. The materials are discussed in Chapter III. As the radius of the cylinder expands, the resonant frequency decreases.

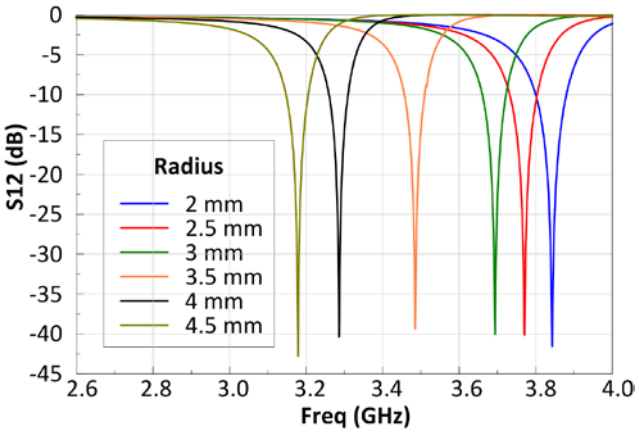

Fig. 2.10. Simulated S12 versus dispersion radius for infinite array.

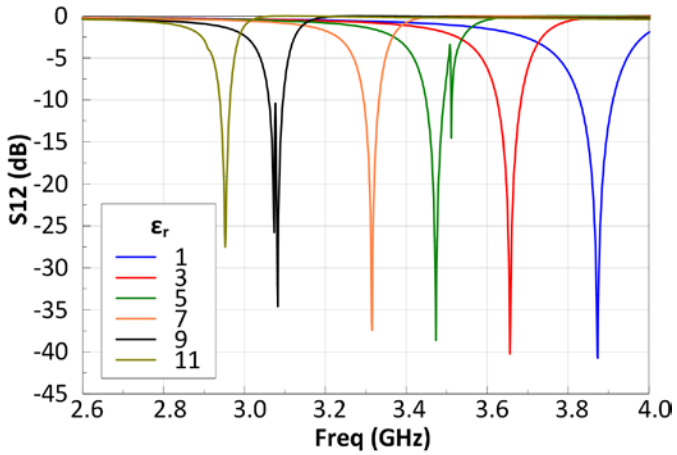

Fig. 2.11. Simulated S12 versus dispersion relative permittivity for infinite array.

When the relative permittivity of the cylinder's material increases the resonant frequency decreases. This relationship can be seen in Figs. 2.12-2.13. Changing the permittivity of the cylinder produces a slightly greater shift than changing the radius of the cylinder.

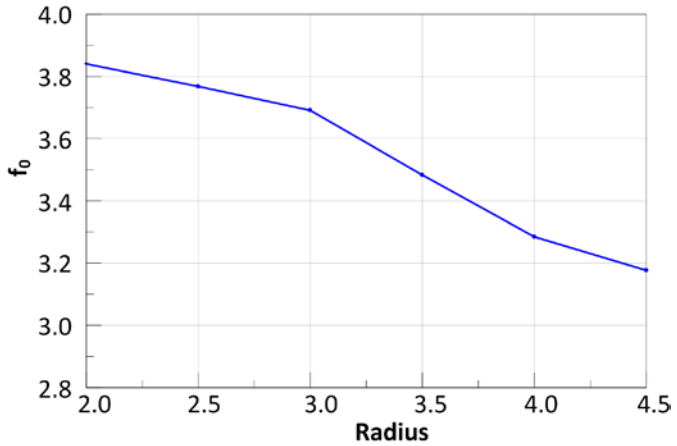

Fig. 2.12. Resonant frequency versus dispersion radius.

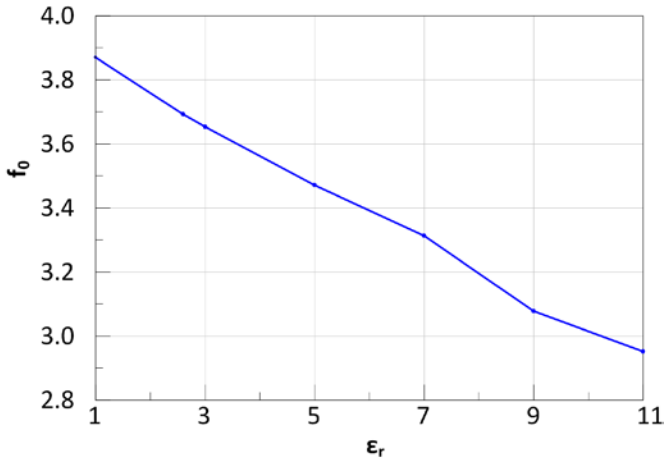

Fig. 2.13. Resonant frequency versus dispersion relative permittivity.

Three experiments are performed to test the capability of tuning this FSS. The first and second experiments are static tests. An array of 3 by 7 spirals is used in the first test. An array of 8 by 8 spirals is used in the second test. A fluidic network is constructed to direct fluid above spirals of an 8 by 8 array for the third experiment. A criterion of stopband strength is specified before the experiments are performed. In order for the stop-band to be considered functional it must reach a -10dB strength. All resonant frequencies are measured from the middle of this -10dB point.

CHAPTER III

MATERIALS

Three materials are utilized as dispersions for tuning the FSS: PDMS, BSTO, and Silicone Oil. Both Silicone Oil and PDMS dispersions are used in the 3 by 7 array static experiment. BSTO is mixed also with PDMS at 40% volume fraction to increase permittivity of the dispersions. Dispersions are fabricated from PDMS and BSTO dispersed in PDMS at 25% and 40% volume fraction for the 8 by 8 array static test. The fluidic network uses Silicone Oil and BSTO dispersed in Silicone Oil at 10%, 20%, 30%, and 40% volume fractions.

Material Properties

The BSTO dispersions are characterized using the Maxwell-Garnett (MG) mixing rule. The dispersions are composed of a fluidic medium (Silicone Oil or PDMS) and inclusions particles (BSTO). As the volume fraction of these particles vary, the material properties of the dispersions change. Permittivity increases when the volume fraction increases. Capacitance is proportional to the permittivity. Resonant frequency decreases as the capacitance increases. The MG rule is dependent on particle geometry as seen in Fig. 3.1. Spherical particles result in smaller changes in material properties unless sufficiently high volume fractions occur in a Polydispersed inclusion (using smaller spheres to fill gaps). More exotic particle shapes such as discs and needles result in larger changes in material properties and achieve higher permittivities with relatively low volume fractions. Unfortunately, BSTO are spherical particles. This is a

disadvantage for a fluidic network. High volume fractions result in very thick mixtures with considerable settling. Lower volume fractions must be used to avoid an overly thick solution. This means less permittivity and less frequency shift.

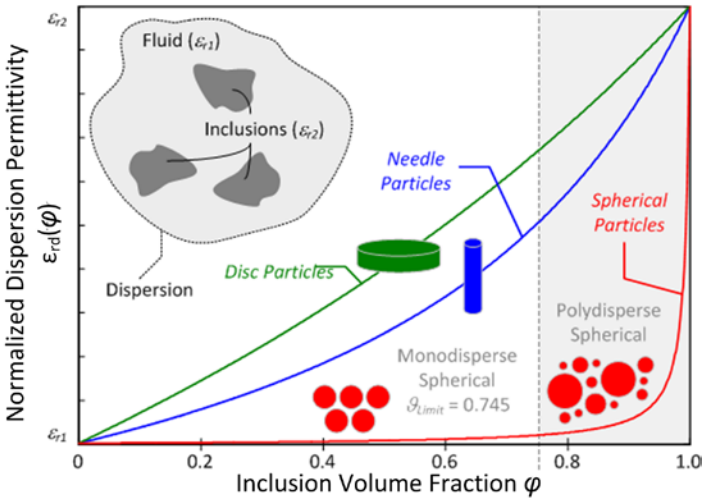

Fig. 3.1. Plot of Maxwell-Garnett mixing rule for various particle geometries.

The dielectric properties of the dispersions are measured using a dielectric probe. The PDMS has an average relative permittivity of 2.634 and the Silicone Oil has an average relative permittivity of 2.750 for 2.6 – 4.0 GHz. The dispersion permittivity, ε_{reff}, is calculated when the relative permittivities of the fluid, ε_{r1}, and BSTO inclusion particles, ε_{r2}, are placed into the MG formula (Eq. 3.1). The symbol, φ, represents the volume fraction of the inclusion particles in the fluid.

$$\varepsilon_{reff} = \varepsilon_{r1} + \frac{3\varphi\varepsilon_{r1}(\varepsilon_{r2} - \varepsilon_{r1})}{\varepsilon_{r2} + 2\varepsilon_{r1} - \varphi(\varepsilon_{r2} - \varepsilon_{r1})} \tag{3.1}$$

Table 3.1 shows the results from the calculations compared to measurements taken from the COSMIX for various volume fractions of BSTO in Silicone Oil. Only

calculations for BSTO dispersed in PDMS can be considered at this time because measurements are not available. The calculated values for BSTO dispersed in PDMS at 25% and 40% volume fraction are 5.213 and 7.766 respectively. While losses can be measured with the dielectric probe, they are not accurate.

Table 3.1
Calculated and Measured εr for Various Volume Fractions of BSTO in Silicone Oil

φ BSTO in Silicone Oil	**10%**	**20%**	**30%**	**40%**
Calculated ε_r	3.650	4.771	6.204	8.102
Measured ε_r	3.587	4.465	5.803	8.404

Dispersion Fabrication

PDMS dispersions for the static experiments are made by punching varying sizes of discs out of sheets of PMDS. The sheets of PDMS are created by pouring thin layers of uncured PDMS into metal trays and allowing it to dry. Cake tips are chosen to punch the discs from the sheets because of their convenient diameters. Three diameters of cake tips are chosen: 5, 6, and 7 millimeters. The cake tips are shown in Fig. 3.2.

Fig. 3.2. Cake tips used for punching out PDMS discs.

Foam trays are created to contain the Silicone oil dispersions above each spiral in the 3 by 7 array experiments. Holes of varying sizes are milled out of adhesive foam sheets as seen in Fig. 3.3. The foam trays are adhered to the top of the FSS and Silicone is placed into the holes.

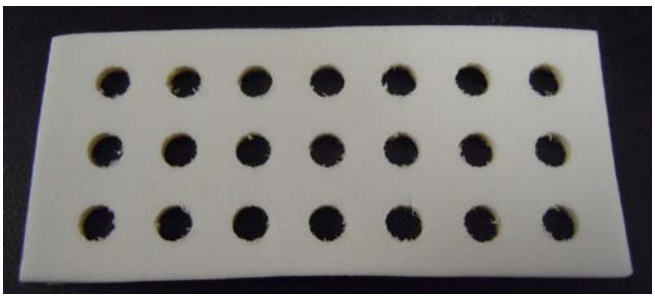

Fig. 3.3. Foam tray for Silicone Oil dispersions.

Fabrication of the fluidic network is discussed in Chapter VI.

CHAPTER IV

STATIC TUNING: 3 BY 7 ARRAY

The first set of static experiments uses an array of 3 by 7 spirals. This creates a surface with dimensions of 30 by 70 millimeters, or 1.181 by 2.756 inches. Three types of materials are used in this set of experiments: PDMS, BSTO dispersed in PDMS at 40 percent volume fraction, and Silicone Oil.

Simulations

The setup is simulated in HFSS before the experiments are performed. PDMS discs are simulated by creating cylinders above each spiral with a relative permittivity of 3. The BSTO dispersed PDMS discs are simulated by increasing the relative permittivity of the discs to 8. A block of air is placed below the FSS to simulate the foam support that will hold the FSS in place while being tested. The disc sizes are increased and decreased using a parametric sweep. The simulated surfaces are shown in Figs. 4.1-4.2.

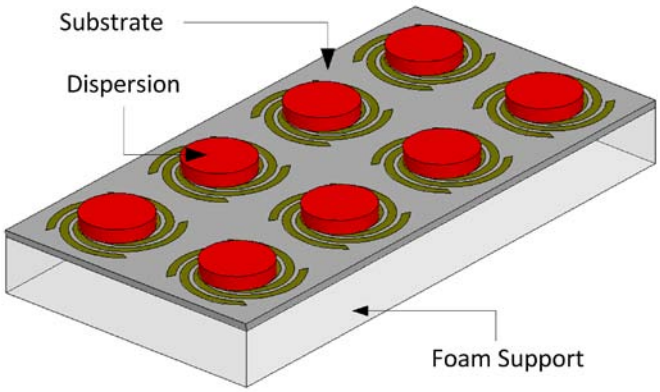

Fig. 4.1. HFSS simulated 4 by 8 array with PDMS discs and symmetry boundaries.

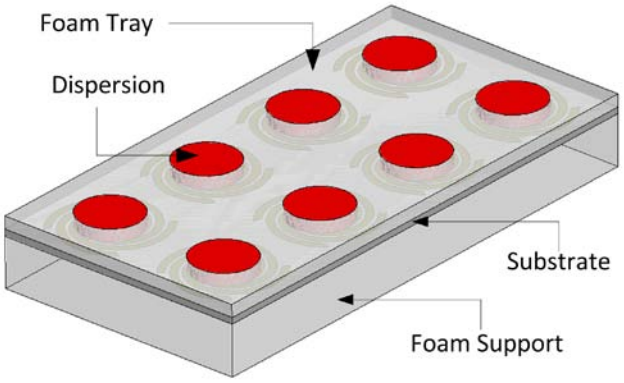

Fig. 4.2. HFSS simulated 4 by 8 array with silicone oil dispersions, foam tray, and symmetry boundaries.

A symmetry boundary is used on a two by four array to reduce run time. No losses are accounted for in these simulations. The results from the HFSS simulations are shown below in Figs. 4.3-4.5. The 4 by 8 simulated array has a resonant frequency of 3.96 without dispersions. A frequency shift occurs as the diameter of each material increases.

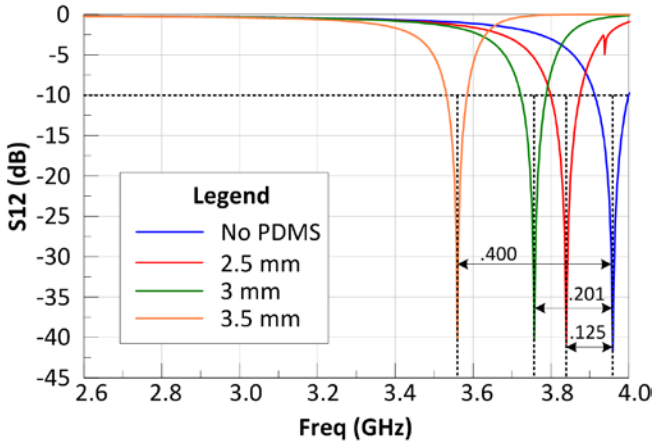

Fig. 4.3. Simulated S12 for 4 by 8 FSS with PDMS discs.

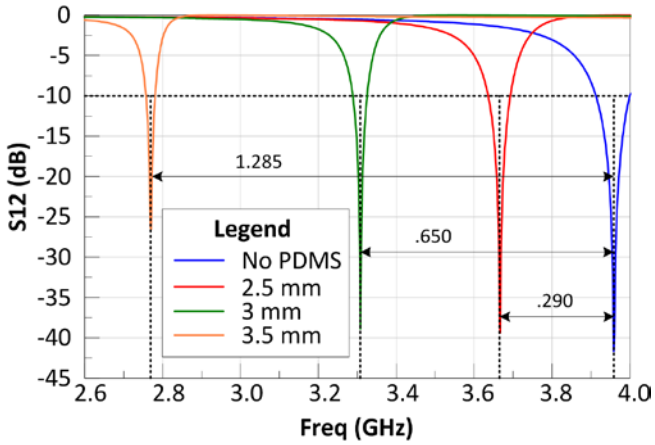

Fig. 4.4. Simulated S12 for 4 by 8 FSS with BSTO in PDMS discs at φ=40%.

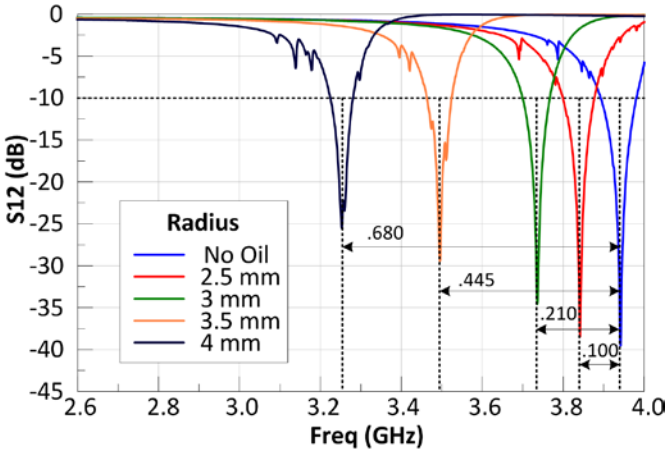

Fig. 4.5. Simulated S12 for 4 by 8 FSS with Silicone Oil dispersions.

Experimental Results

The 3 by 7 FSS is etched onto a 20 mil sheet of Duroid 5880. The final 3 by 7 array is shown below in Fig. 4.6.

Fig. 4.6. 3 by 7 FSS.

Fig. 4.7 shows the FSS with the three types of dispersions: PDMS, BSTO dispersed in PDMS, and the foam tray that will hold the Silicone oil.

Fig. 4.7. 3 by 7 FSS with PDMS discs(top), BSTO in PDMS discs at φ=40%(middle), Silicone Oil foam tray(bottom).

The FSS is placed between two S-band coax-to-waveguide adapters with dimensions of 1.340 by 2.840 inches for testing. The adapters work in the frequency range 2.6 to 3.95 GHz. Fig. 4.8 shows the test setup with the coax to waveguide adapters. The FSS is supported by a piece of foam.

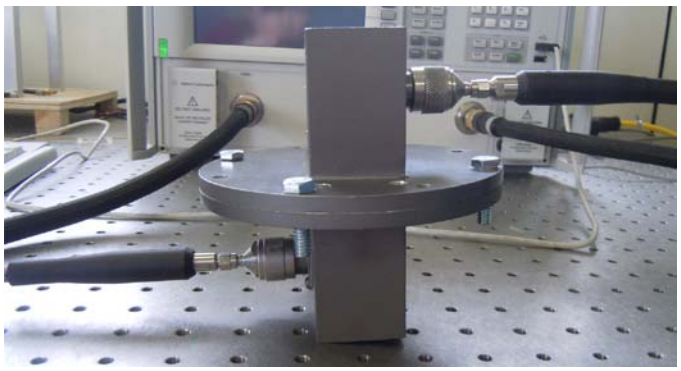

Fig. 4.8. Test setup for 3 by 7 FSS experiments.

The 3 by 7 FSS has a resonant frequency of 3.95 GHz as seen in Fig. 4.9. This resonant frequency is slightly higher than that of the simulated infinite array. However, the resonant frequency is very close to the expected value of 3.96 GHz when compared to the simulated 3 by 7 array.

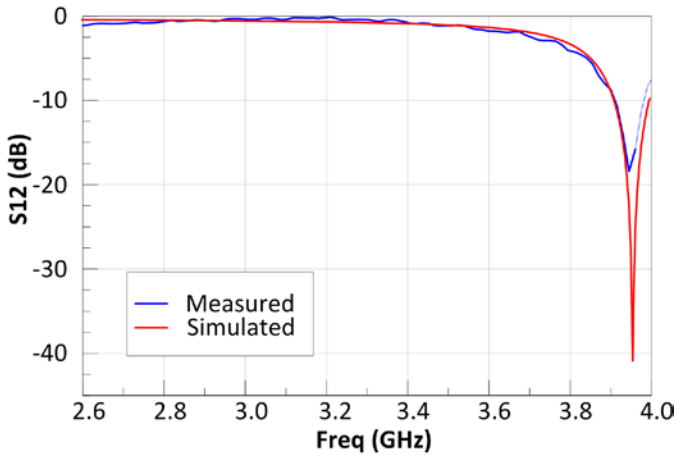

Fig. 4.9. Comparison of simulated and measured S12 for 3 by 7 FSS.

The resonant frequency shifts lower as expected when the PDMS discs are added. The 3.5 mm discs did not meet the -10 dB criteria for operation. The results can be seen in Fig. 4.10.

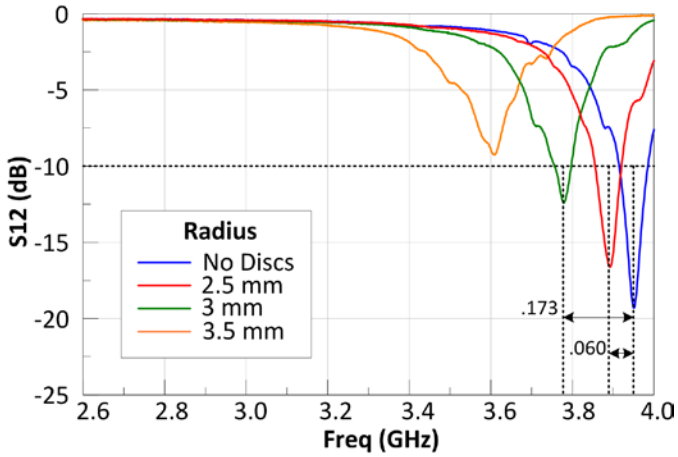

Fig. 4.10. Measured S12 for 3 by 7 FSS with PDMS discs.

The PDMS discs do not achieve the magnitude of shift that was seen in simulations. The stop-bands also lose their strength as the dispersions increase. Reasons for this lack of shift and loss of strength are discussed in Chapter V under Errors and

Losses. Fig. 4.11 shows a comparison of S11 and S12 for the FSS with and without dispersions.

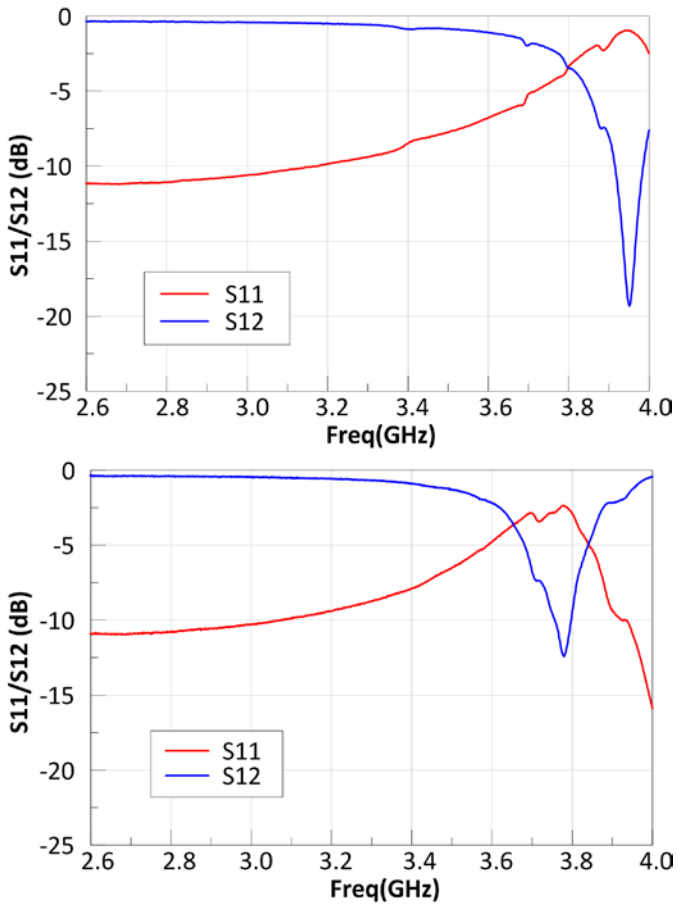

Fig. 4.11. Comparison of measured S11/S12 for 3 by 7 FSS with and without PDMS discs.

The BSTO discs achieved a greater shift in resonant frequency for the 2.5 mm and 3 mm discs as seen in Fig. 4.12. The 3.5 mm discs did not meet the -10 dB requirement.

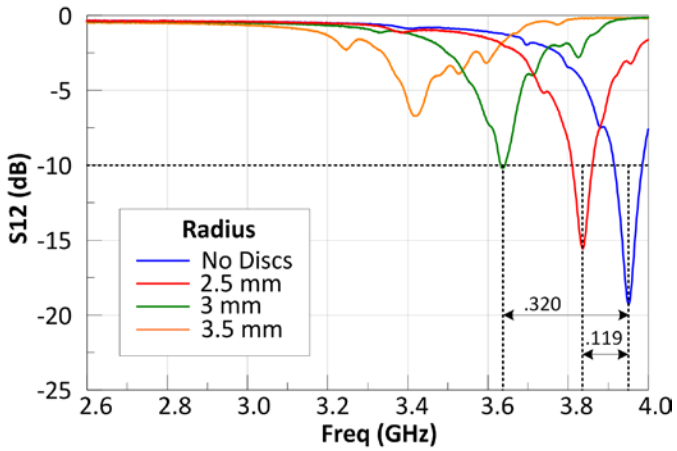

Fig. 4.12. Measured S12 for 3 by 7 FSS with BSTO in PDMS discs at φ=40%.

The Silicone Oil achieved the best shift in resonant frequency for the 3 by 7 array. Fig. 4.13 shows the results for this test. The 4 mm curve did not meet the -10 dB limit due to the shape of the curve. This is due to inconsistent filling of reservoirs. A maximum shift of .699 GHz was achieved with the 5mm dispersions. This more than doubles the results from the PDMS and BSTO results.

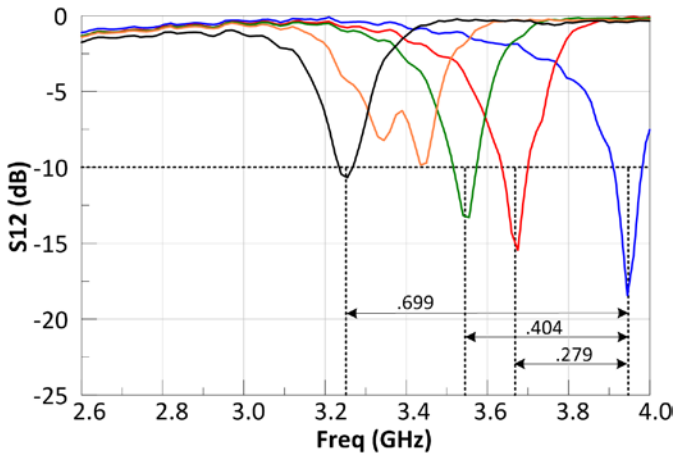

Fig. 4.13. Measured S12 for 3 by 7 FSS with Silicone Oil dispersions.

The foam trays attached to the FSS had a small impact on the magnitude of shift achieved in Fig. 4.13. Figs. 4.14-4.15 show the effect of adding the foam trays. Fig. 4.14 shows the shift seen by adding the 2 mm foam cover and then adding the Silicone oil. Fig. 4.15 compares the shifts from each foam cover.

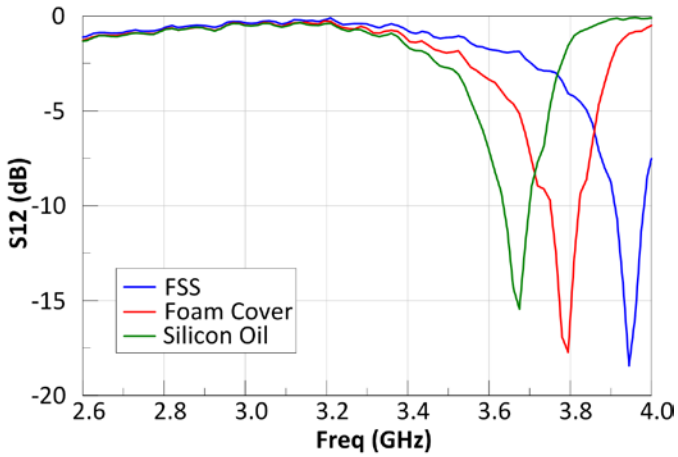

Fig. 4.14. Measured S12 for 3 by 7 FSS with no dispersion, 2 mm foam tray, and 2 mm Silicone Oil dispersion.

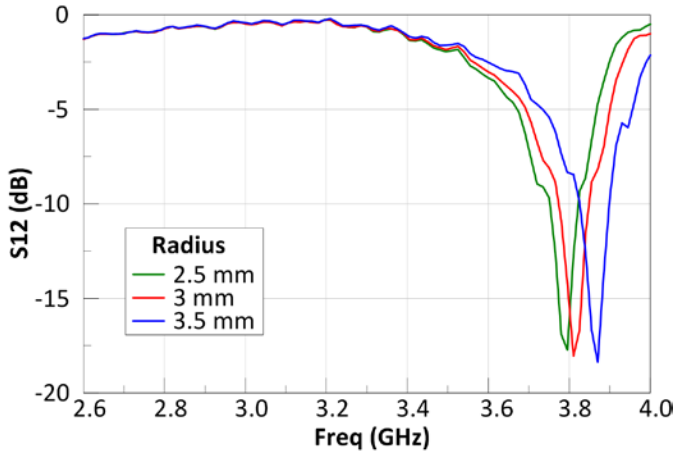

Fig. 4.15. Comparison of measured S12 for 3 by 7 FSS with various foam trays.

CHAPTER V

STATIC TUNING: 8 BY 8 ARRAY

An array of 8 by 8 spirals is used in the second set of static experiments. This creates a surface with dimensions of 80 by 80 millimeters, or 3.150 by 3.150 inches. A square surface was chosen for this experiment for rotational symmetry and to demonstrate independence between TE and TM waves. Two types of materials are used for the 8 by 8 array experiments: PDMS and BSTO dispersed in PDMS at 25% and 40% volume fraction.

Expanded Waveguide

An expanded square waveguide was constructed for testing with the same inner dimensions as the FSS: 80 by 80 millimeters. Each section of the expanded waveguide is 150 mm long. The FSS is placed between the two sections of waveguide. The same S-band adapters from the previous experiment are used to connect the square waveguide sections to the network analyzer cables. Fig. 5.1 shows the setup for this experiment. The discontinuity between the adapters and the square waveguides creates an iris and produces an unwanted reflection. This reflection can be seen in Fig. 5.2.

Fig. 5.1. Expanded waveguide.

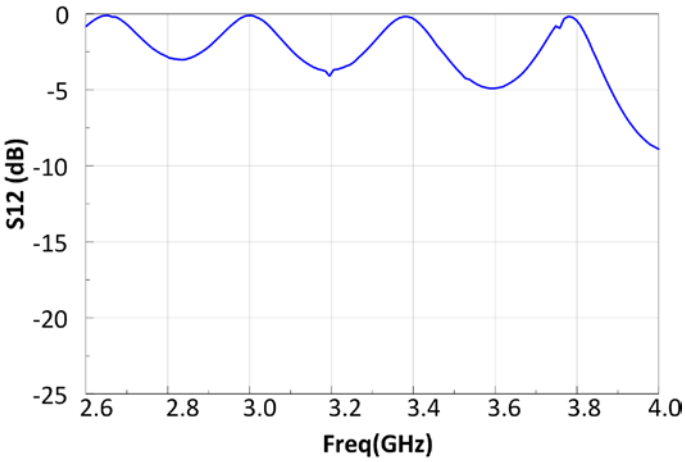

Fig. 5.2. Measured S12 for expanded waveguide before calibration.

The reflection can be removed with a TRL calibration. A new section of waveguide is made with the same dimensions as the two previous sections: 80 mm by 80 mm and 150 mm long. A short plate is also made to fit the aperture of the waveguide. The calibration procedure is set up on the network analyzer. Calibrated waveguide signal is shown in Fig. 5.3.

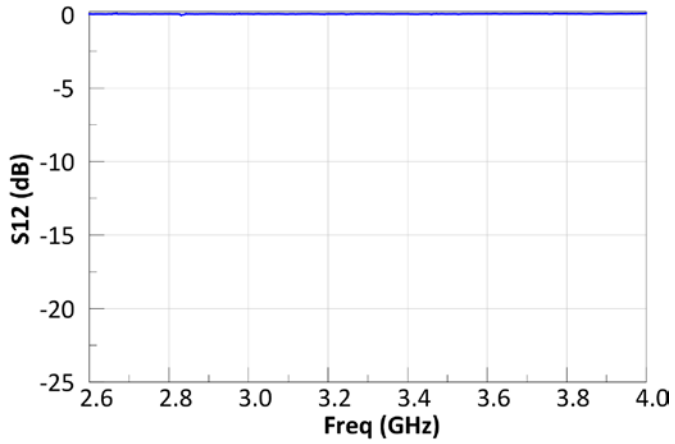

Fig. 5.3. Measured S12 for expanded waveguide after calibration.

Simulations

The FSS is simulated in HFSS before the experiments are performed. The waveguide to adapter discontinuity is accounted for in this simulation. A block of air is placed below the FSS to simulate the foam support block that will hold the FSS in place while being tested. A symmetry boundary is used on a four by four array to reduce run time. The results from the HFSS simulations are shown below in Fig. 5.4. The 8 by 8 array has a resonant frequency of 3.96 GHz without dispersions.

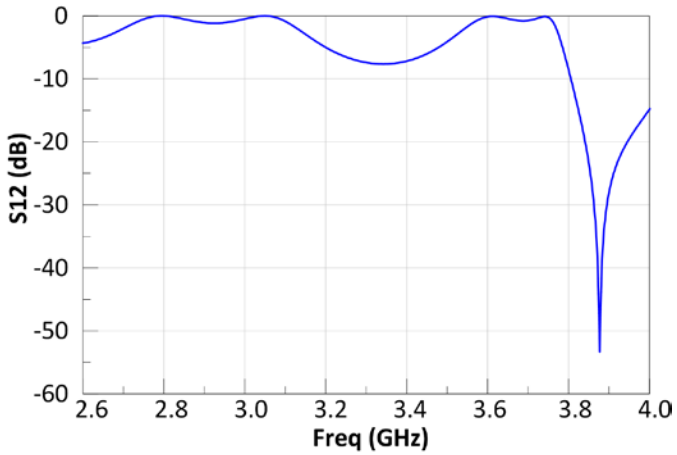

Fig. 5.4. Simulated S12 of 8 by 8 FSS in non-calibrated waveguide.

Simulations with the dispersions are not obtained. The problem is very large for HFSS and has difficulty converging.

Experimental Results

The 8 by 8 FSS is etched onto a 20 mil sheet of Duroid 5880. The final array is shown below in Fig. 5.5.

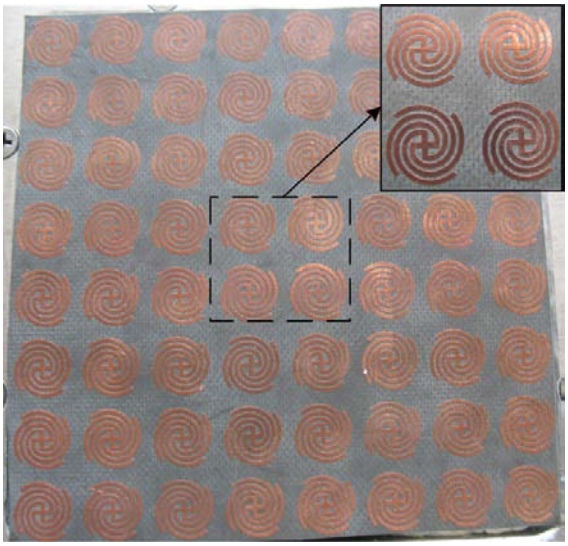

Fig. 5.5. 8 by 8 FSS with close up of spirals.

Fig. 5.6 shows the FSS with the three types of dispersions: PDMS and BSTO dispersed in PDMS at 25% and 40% volume fraction.

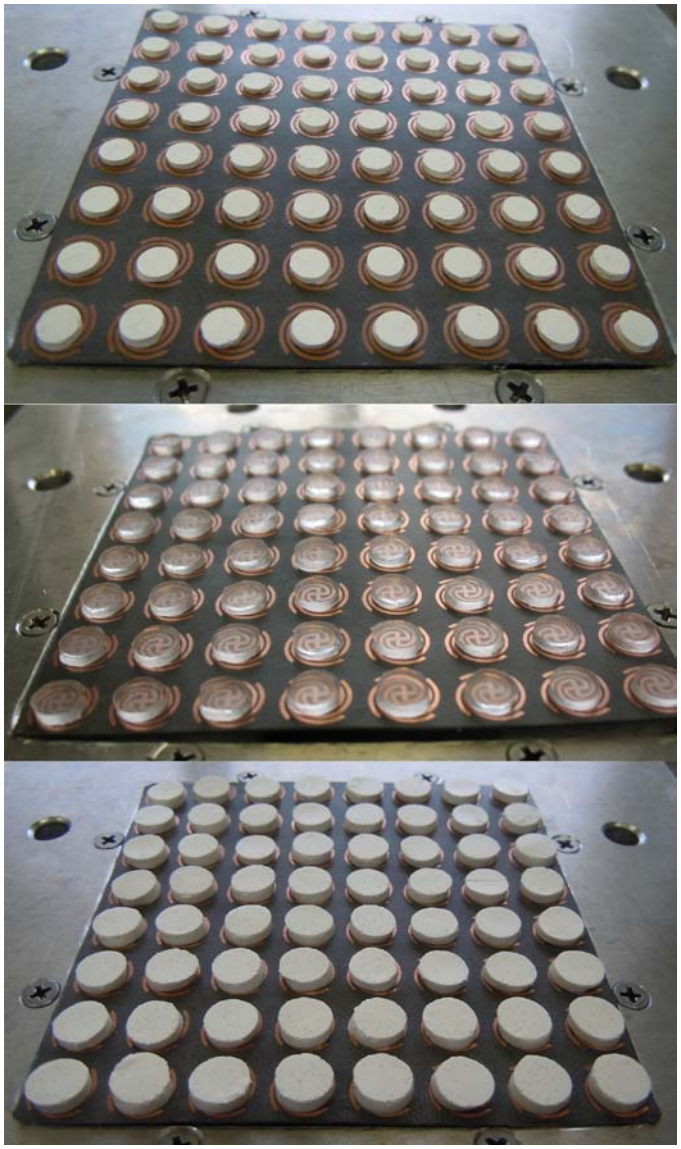

Fig. 5.6. 8 by 8 FSS with BSTO in PDMS discs at φ=40%(top), PDMS discs(middle), BSTO in PDMS discs at φ=25%(bottom).

The 8 by 8 FSS has a resonant frequency of 3.861 GHz without calibrations as seen in Fig. 5.7. This resonant frequency is slightly lower than that of the simulated

infinite array. However, the resonant frequency is very close to the expected value of 3.960 GHz when compared to the simulated 8 by 8 array.

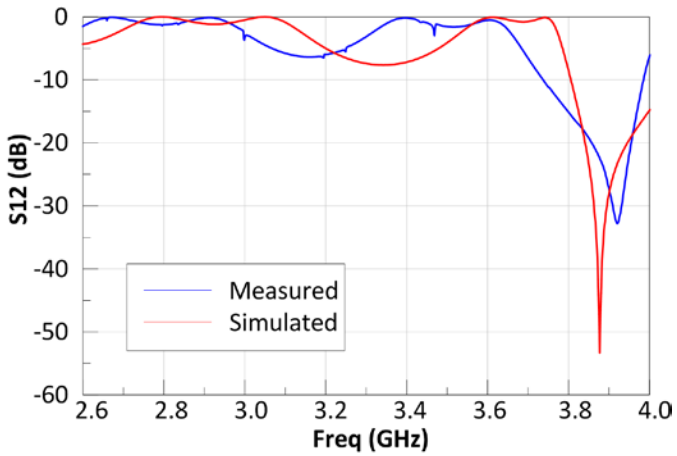

Fig. 5.7. Comparison of simulated and measured S12 for 8 by 8 FSS.

The new measured resonant frequency of the FSS is 3.910 GHz when the waveguide is calibrated. A comparison of the calibrated versus non-calibrated system is shown in Fig. 5.8.

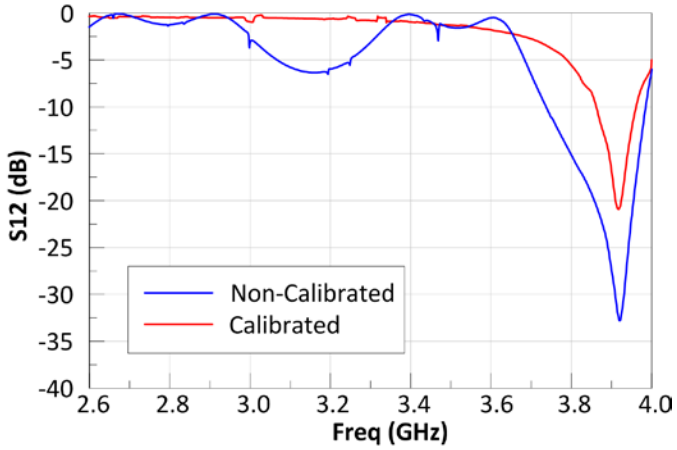

Fig. 5.8. Comparison of measured S12 for 8 by 8 FSS in calibrated and non-calibrated waveguide.

A small amount of noise occurs in the transmission plot after the calibration. The use of smoothing eliminates the noise in the plot but also decreases the power of the stopband. A comparison of the smoothed and non-smoothed signal from the FSS is shown in Fig. 5.9. All measurements will be smoothed to reduce noise.

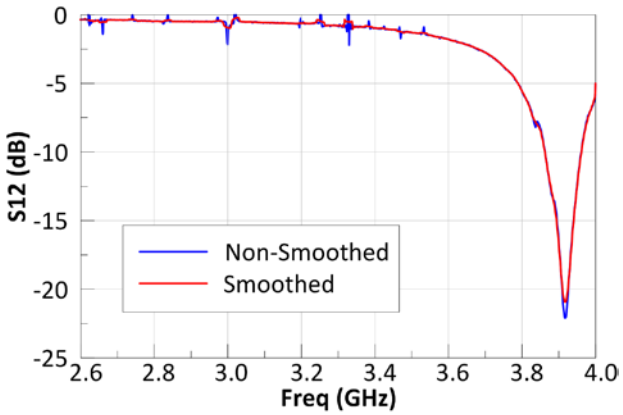

Fig. 5.9. Comparison of smoothed and non-smoothed S12 for 8 by 8 FSS.

The resonant frequency shifts lower as expected when the PDMS discs are added. The results can be seen in Fig. 5.10. The shifts are very similar in magnitude to the shifts from the 3 by 7 array.

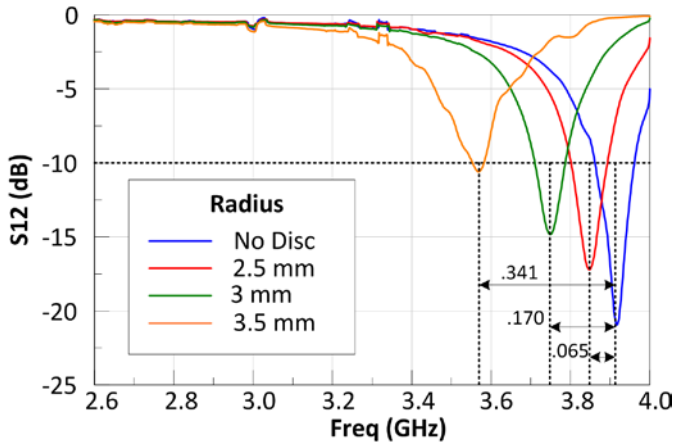

Fig. 5.10. Measured S12 for 8 by 8 FSS with PDMS discs.

The 25% BSTO discs achieved a greater shift in resonant frequency as seen in Fig. 5.11. However, the 3.5 mm discs did not meet the -10dB criteria.

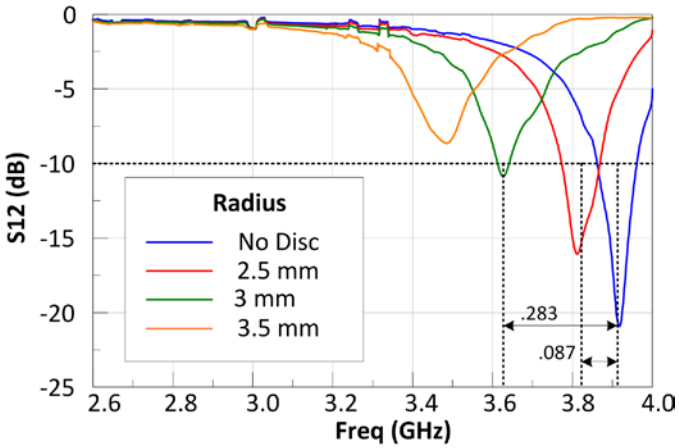

Fig. 5.11. Measured S12 for 8 by 8 FSS with BSTO in PDMS discs at φ=25%.

The 40% BSTO discs achieved an even greater shift in resonant frequency than the two previous materials as seen in Fig. 5.12. The 3.5 mm discs did not meet the -10dB criteria again.

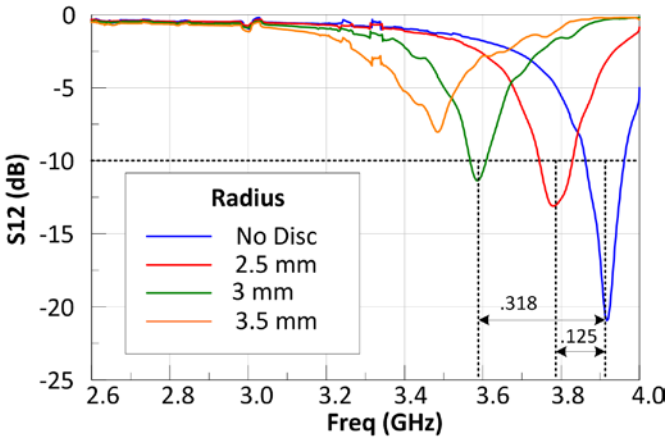

Fig. 5.12. Measured S12 for 8 by 8 FSS with BSTO in PDMS discs at φ=40%.

Windowing

Previous static tests confirm the ability to tune the resonant frequency using dispersions of varying size and material. The next step is to determine whether multiple "windows", or stop-bands, can be achieved at one instance by loading groups of spirals within the FSS with dispersions. The 3 mm PDMS discs are used in this experiment.

The first pattern to be tested is one outer row of the FSS. An image of this pattern is seen in Fig. 5.13. The choice of outer row is dependent upon the polarization of the wave. The row must be perpendicular to the E field to produce the optimum windowing effect. This positioning allows the effect of the dispersions to be added. Fig. 5.14 reveals two resonance frequencies being excited. The largest band-stop peak in insertion loss (IL) represents the spirals that are not covered with PDMS discs. This stop-band is much stronger because there are more uncovered spirals. The resonant frequency of this stop-band is 3.910 GHz. This is consistent with the originally measured resonant frequency of the FSS as seen in Fig. 5.12. The second stop-band occurs at about 3.750 GHz. This is consistent with the position of the stop-band produced by the 3 mm PDMS

discs in Fig.5.10. A stop-band at around 3.740 GHz is observed when the 3 mm PDMS discs completely cover the 8 by 8 array.

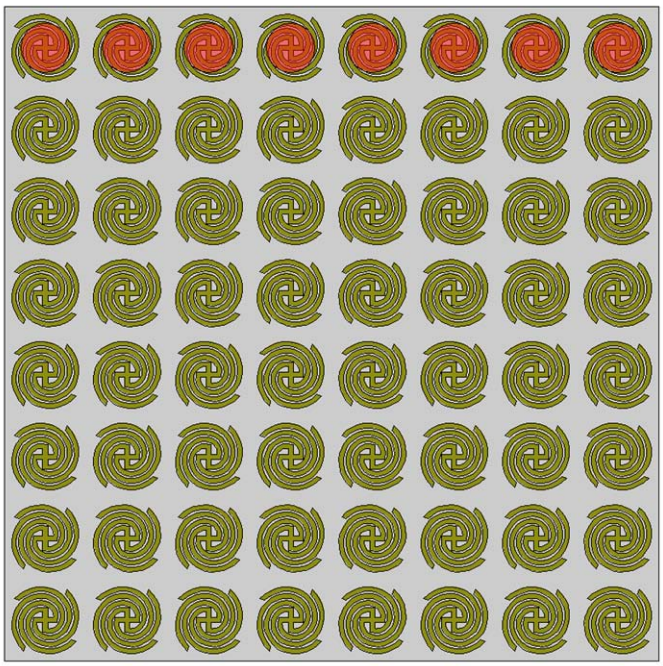

Fig. 5.13. Image of 8 by 8 FSS with one row of spirals loaded with PDMS discs.

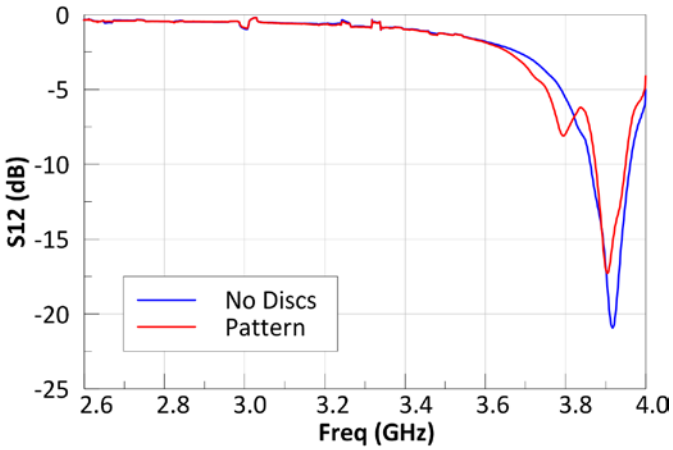

Fig. 5.14. Measured S12 for 8 by 8 FSS with one row of spirals loaded with PDMS discs.

The next pattern to be tested is half of the FSS. Fig. 5.15 shows this pattern. The results are shown in Fig. 5.16. The optimum windowing is achieved when more of the dispersions are aligned perpendicular to the E-field similar to the previous experiment. However, each rotation achieves similar results because the structure is split evenly. Two resonant frequencies are distinguished. The left peak in IL, representing the uncovered spirals, is at 3.910 GHz. The right peak in IL, representing the covered spirals, is at 3.750 GHz. The two resonant frequencies are identical to the two resonant frequencies found in the previous pattern.

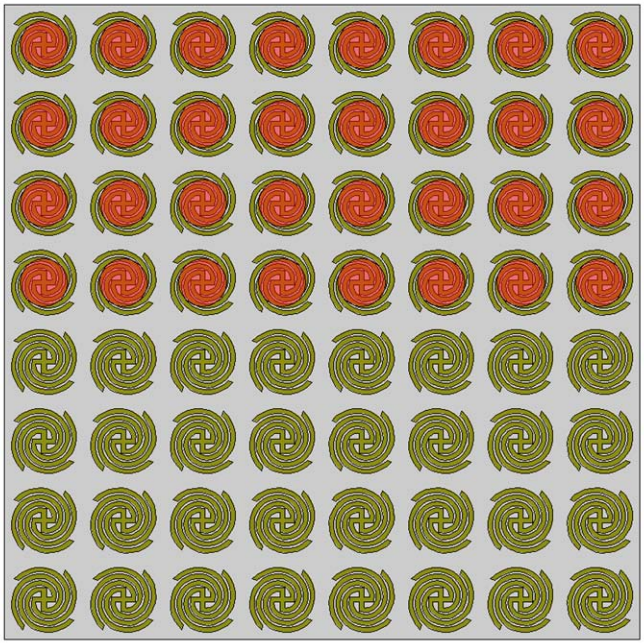

Fig. 5.15. Image of 8 by 8 FSS with half of spirals loaded with PDMS discs.

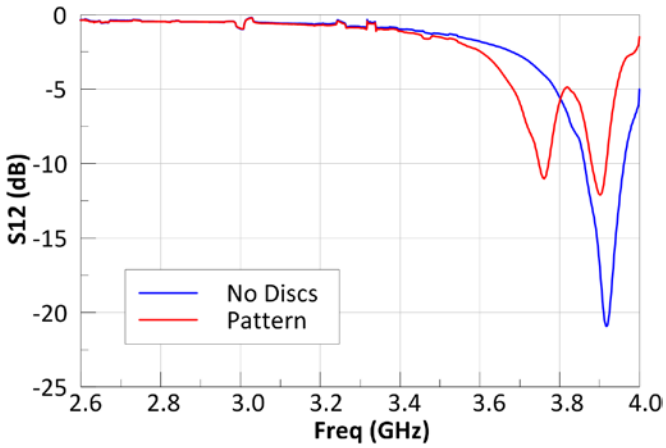

Fig. 5.16. Measured S12 for 8 by 8 FSS with half of spirals loaded with PDMS discs.

The third pattern is shown in Fig. 5.17. A little more than half of the FSS is covered: 36 out of 64 spirals. The lower stop-band is stronger because the number of covered spirals now exceeds the number of uncovered spirals. Rotation of the FSS is negligible due to symmetry of the pattern. The results are shown in Fig. 5.18. The right peak in IL represents the uncovered spirals at 3.910 GHz. The left peak in IL represents the covered spirals at 3.750 GHz. Again, the two resonant frequencies are identical to the two resonant frequencies found in the previous pattern.

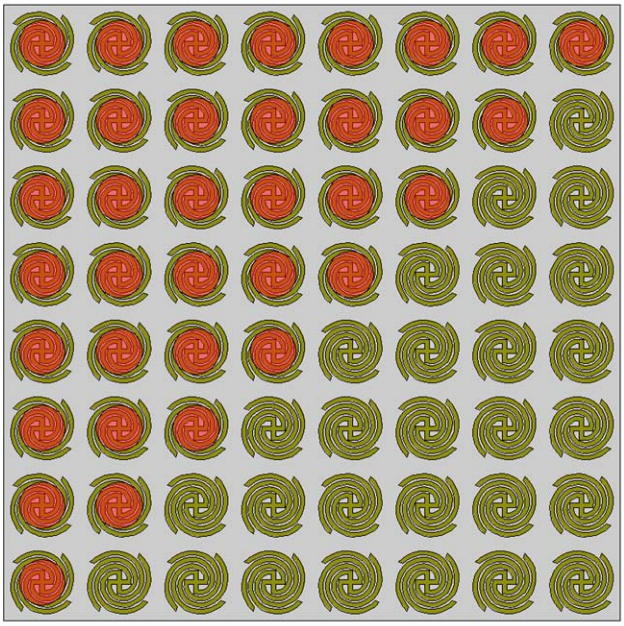

Fig. 5.17. Image of 8 by 8 FSS with diagonal half of spirals loaded with PDMS discs.

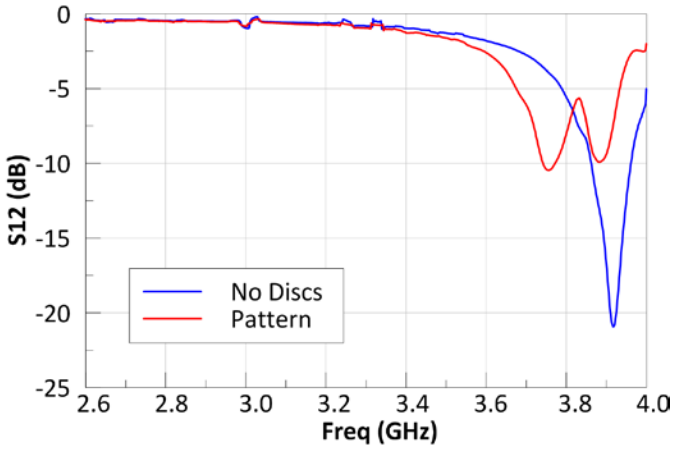

Fig. 5.18. Measured S12 for 8 by 8 FSS with diagonal half of spirals loaded with PDMS discs.

The final pattern to be tested is the same pattern that will be used for the fluidic network. The middle 16 spirals are covered with PDMS discs. Orientation with respect to polarization is negligible because the structure appears the same from each side. Fig. 5.19 shows this pattern. The results from this measurement are shown in Fig. 5.20. The

left peak in IL, representing the uncovered spirals, is at 3.910 GHz. The right peak in IL, representing and the covered spirals, is at 3.750 GHz. The two resonant frequencies are consistent with expected frequencies.

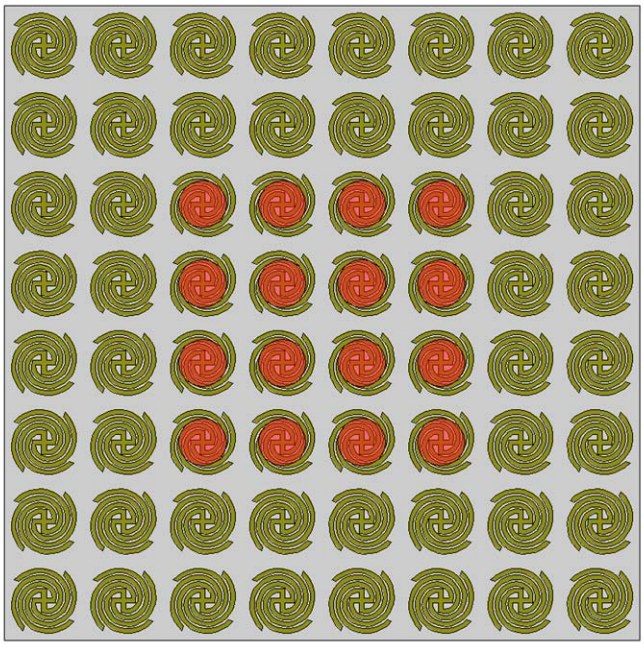

Fig. 5.19. Image of 8 by 8 array with middle 16 spirals loaded with PDMS discs.

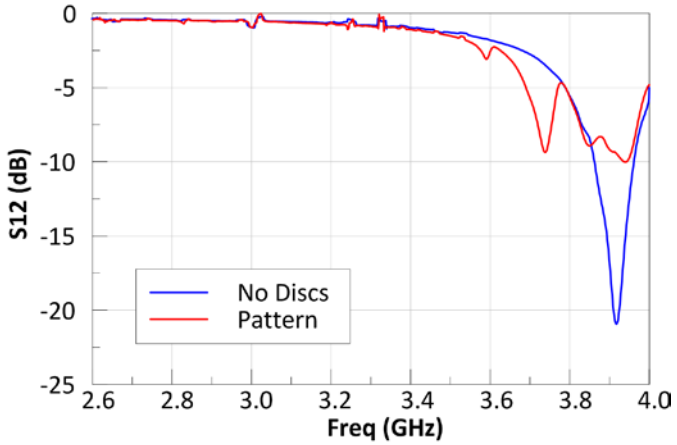

Fig. 5.20. Measured S12 for middle 16 spirals of 8 by 8 FSS loaded with PDMS discs.

CHAPTER VI

ERRORS AND LOSSES

Errors and losses have a large impact on the ability to tune the FSS. Two forms of human errors in this experiment are fabrication of discs and placement of discs.

Disc sizes can vary from fabrication errors. The cake tips slightly bend while punching discs from sheets of PDMS. This causes each disc to have a unique shape and size. Variation in disc size causes small changes in the amount of spiral that is covered by each disc. The errors add up to create new resonant frequencies or widening of the stop-band. Disc thickness also varies. The PDMS is poured into trays to dry into sheets. PDMS can shift towards one side and cause the sheet to be uneven if the trays are not level. Discs do not have a uniform thickness when they are punched out of the unlevel sheets. Some spirals are covered with more PDMS than others. This causes varying resonant frequencies.

The placement of discs is also crucial to resonant frequency. The slightest misplacement of a disc can create a new resonant frequency. This also widens the bandwidth of the stop-band. Fig. 6.1 shows a close-up of the loaded FSS. All discs have different shapes and are not all perfectly centered on each spiral. This kind of error can cause strange responses. Figs. 6.2-6.3 show a comparison of the 3 by 7 array PDMS experiment with sloppy placement of discs and precise placement of discs.

Fig. 6.1. Close up of PDMS discs on spirals.

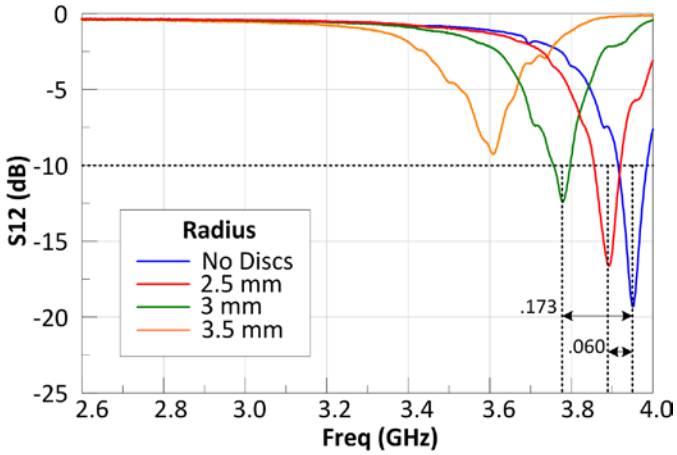

Fig. 6.2. Measured S12 for 3 by 7 array with improved disc placement.

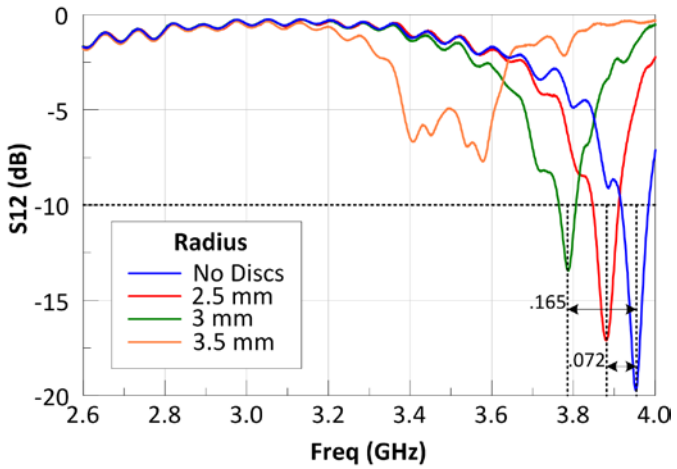

Fig. 6.3. Measured S12 for 3 by 7 array with sloppy disc placement.

A large amount of attention is placed on the positioning of the discs so better results are attained. It is still very difficult to place each disc perfectly in the center of the spirals even with this new focus. Discs can be bumped out of place when the FSS is touched.

The 2.5 mm PDMS discs are placed onto the 8 by 8 array. The array is rotated 360 degrees in the waveguide to observe the impact of disc placement. Fig. 6.4 shows a close up of the stop-band. Every rotation presents a slightly different response while being fairly close to the same resonant frequency.

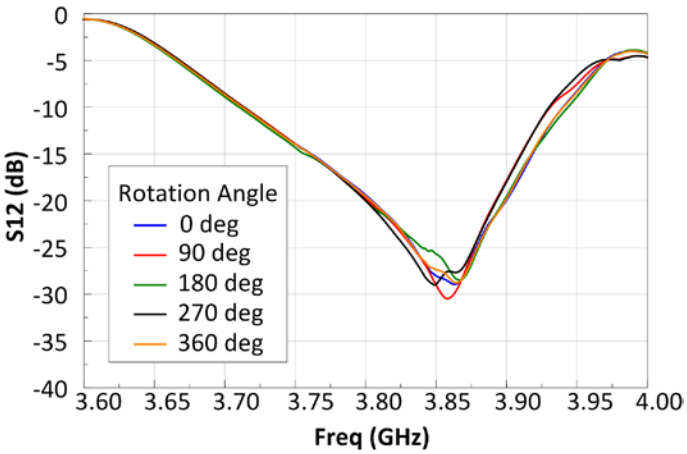

Fig. 6.4. Measured S12 for various rotations of 8 by 8 array in waveguide with PDMS discs.

Losses exist in the materials being used. Losses can be measured with the dielectric probe but are very inaccurate. It is difficult to determine the actual loss of the materials. Simulations can help predict the losses in materials. A simulation without losses and with losses in PDMS is compared. Fig. 6.5 shows a simulation of the FSS loaded with PDMS (ε_r =3) without any loss. There is not deterioration in the stop-band as the radius increases.

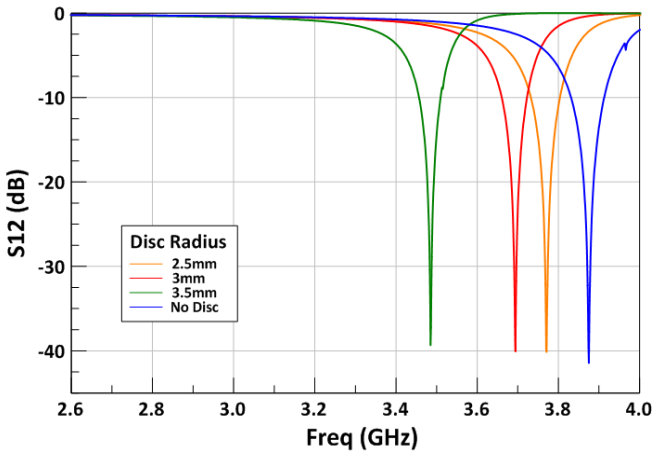

Fig. 6.5. Simulated S12 for FSS with lossless dispersions.

The stop-band begins to lose its strength when losses are added. Fig. 6.6 shows a comparison of the simulation with a loss tangent of .001 compared to measured results from the 8 by 8 array.

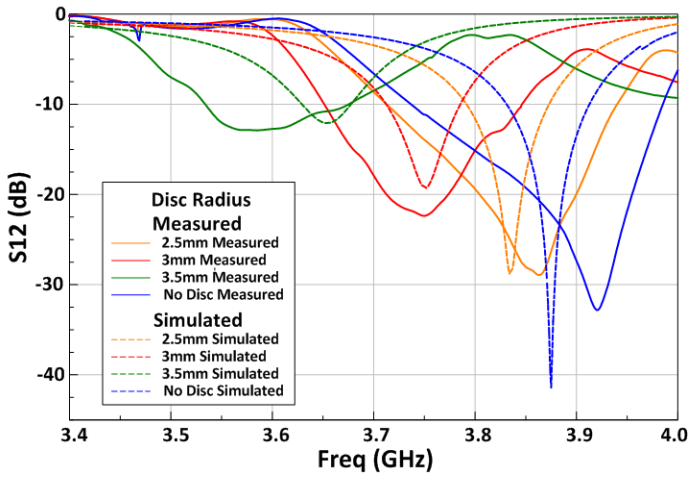

Fig. 6.6. Comparison of measured S12 for 8 by 8 array and simulated S12 for FSS with material losses.

CHAPTER VII

FLUIDIC TUNING

The fluidic network uses Silicone Oil dispersions. Silicone oil is mixed with BSTO at varying volume fractions: 0%, 10%, 20%, 30%, and 40%. This mixture is directed to each spiral through channels. An outlet channel layer allows for the mixture to then be drained out the other side. Fig. 7.1 shows the layout of the fluidic network.

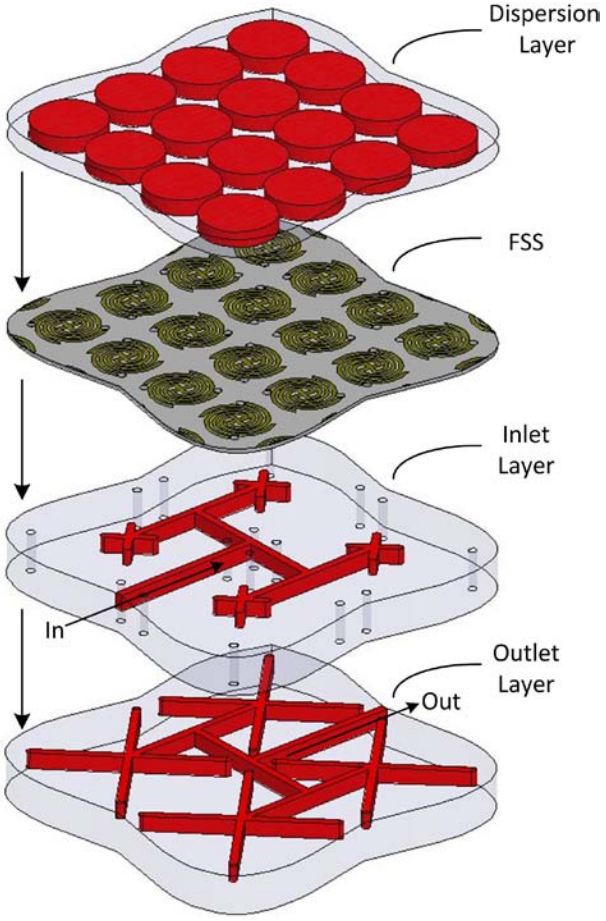

Fig. 7.1. Diagram of fluidic network layers.

The dispersion layer sits above FSS and holds the Silicone Oil mixture. The inlet layer directs fluid to each spiral. The outlet layer drains fluid from each spiral. Holes in FSS allow fluid flow between the dispersion layer and the inlet/outlet layers. Fig. 7.2 shows a close up of the inlet layer. The channels are 1 mm wide and 2mm deep.

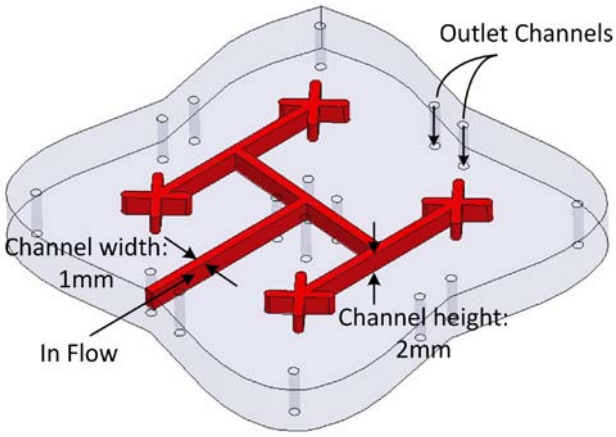

Fig. 7.2. Diagram of fluidic network inlet layer.

The network is tested with the same two sections of square waveguide from the 8 by 8 array. However, the calibration parts were not made before measurements of the fluidic network were taken. The reflection pattern seen in Chapter V is present in the measurements of the fluidic network.

Fabrication

The spirals on the FSS are rotated 10° to align the ends of the spiral arms with the inlet and outlet holes. The rotation prevents drilling into the spiral arms. Fig. 7.3 shows this rotation. Inlet and outlet holes are drilled at the ends of the middle 16 spirals' arms. The holes are drilled using a .0197" drill bit on a milling machine. Fig.7.4 shows a close up of the FSS with the newly drilled holes.

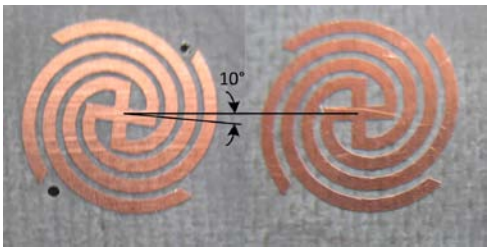

Fig. 7.3. Comparison of original spiral to fluidic network spiral.

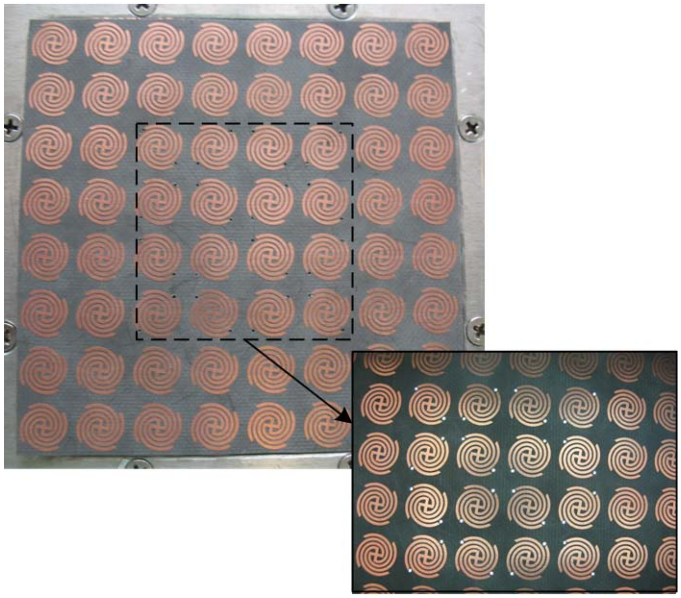

Fig. 7.4. Close up of fluidic network FSS.

The rotation and holes have little effect on the resonant frequency of the FSS. Fig. 7.5 shows a comparison of S12 for the old FSS and the new rotated FSS.

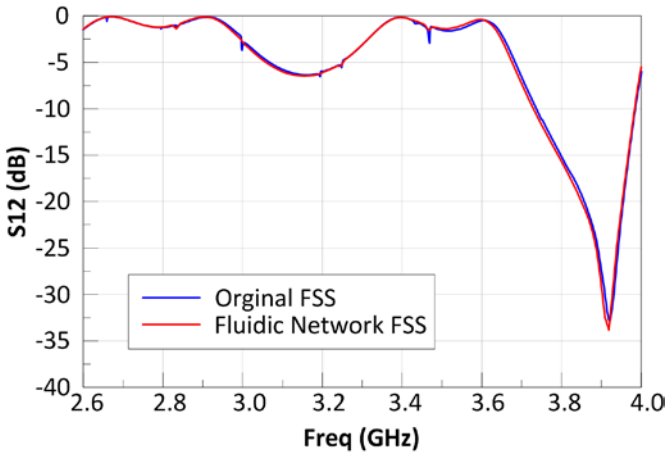

Fig. 7.5. Comparison of measured S12 for original FSS and fluidic network FSS.

The PDMS channel layers are created by pouring PDMS into master molds and allowing it to set. The master molds are created with rapid prototyping machine. The master molds can be seen in Fig. 7.6. Outlet holes are punched into inlet layer using a punch after all the PDMS layers are dry. Fig. 7.2 shows the position of the outlet holes relative to the inlet channels. A thin layer of PDMS is applied to bottom and top of the FSS. Finally, all layers are plasma bonded together.

The device was tested by injecting blue colored alcohol into the inlet and outlet channels. Fig. 7.7 shows the blue fluid flowing through the channels. Bubbles formed in the channels and in the dispersion layer. Slits were cut into the tops of each dispersion cavity to release air bubbles.

Fig. 7.6. Master molds for fluidic network PDMS layers.

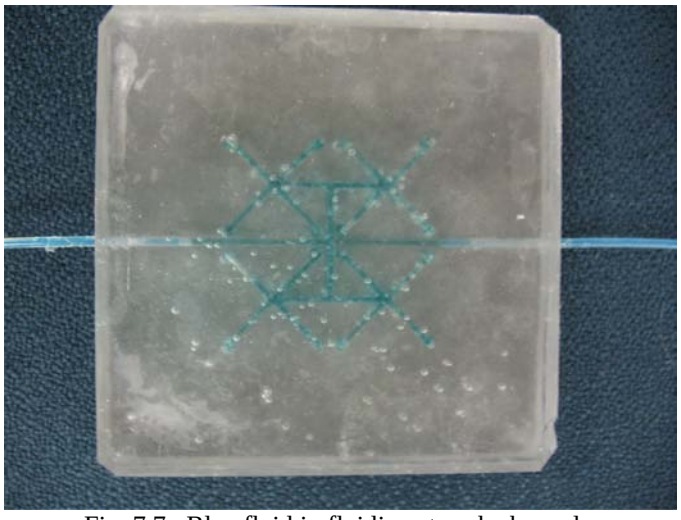

Fig. 7.7. Blue fluid in fluidic network channels.

The injection setup for the fluidic network is seen in Fig. 7.8. A syringe is used to pump the mixture into the inlet channel. The outlet channel drains into a beaker. The tubes are unhooked once each reservoir is filled. The device is placed between the two waveguide sections for testing.

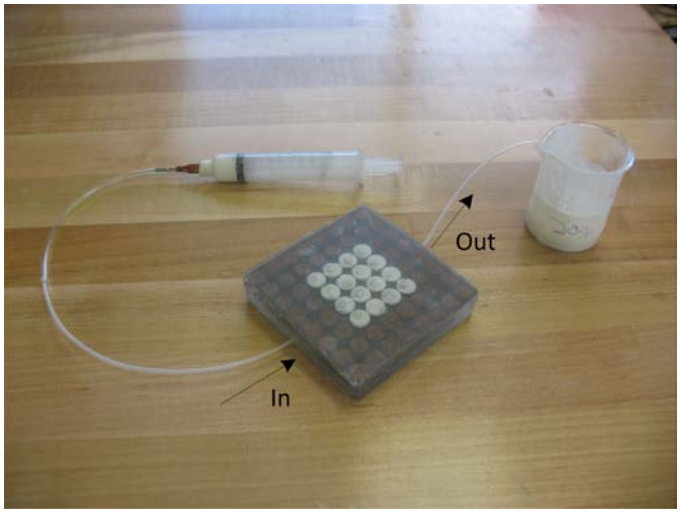

Fig. 7.8. Fluidic network test setup.

Experimental Results

Fig. 7.9 shows the transmission through the network before any mixture is injected into the channels. Two resonant frequencies occur: 3.5 GHz and 3.1 GHz. The 3.1 GHz resonant frequency represents the spirals that are completely covered with PDMS. The 3.5 GHz resonant frequency represents the spirals with dispersion reservoirs above them. The spirals that are beneath the reservoirs have a 1 mm layer of PDMS above them that closes off the reservoir. This causes their resonant frequency to be slightly lower than the original 3.861 GHz. The gaps between each spiral are also

covered by PDMS unlike the static experiments. This causes an even lower resonant frequency to occur.

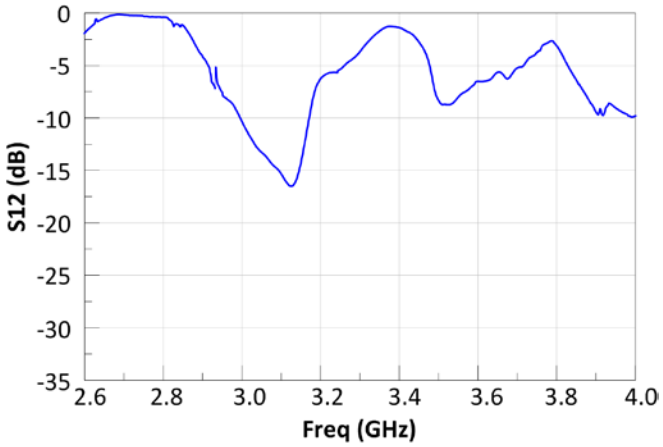

Fig. 7.9. Measured S12 for fluidic network without injected Silicone Oil.

The first injected mixture is Silicone Oil. The results from that injection are shown in Fig. 7.10. Only one resonant frequency can be observed. The strength of the stopband is also stronger than before. Silicone Oil has a relative permittivity very close to PDMS. It is as if the entire structure is covered in a constant relative permittivity with all the reservoirs full of the oil. This completely lowers the resonant frequency of the entire FSS to one unique frequency.

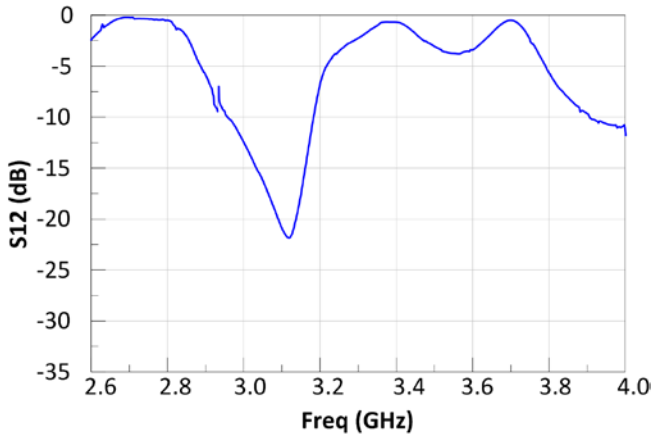

Fig. 7.10. Measured S12 for fluidic network with Silicone Oil.

The next mixture to be injected into the fluidic network is a combination of BSTO in Silicone Oil at 10% volume fraction. The results from this test are shown in Fig. 7.11. Two resonant frequencies appear in this plot. The 10% volume fraction generated a response very similar to the static pattern. This resemblance is shown in Fig. 7.12.

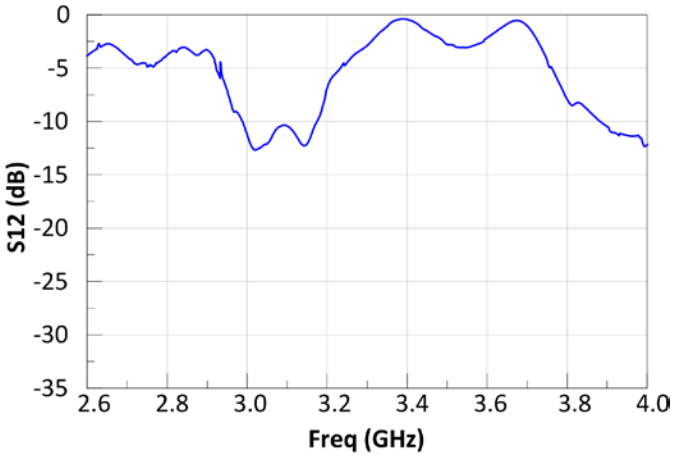

Fig. 7.11. Measured S12 for fluidic network with BSTO in Silicone Oil at φ=10%.

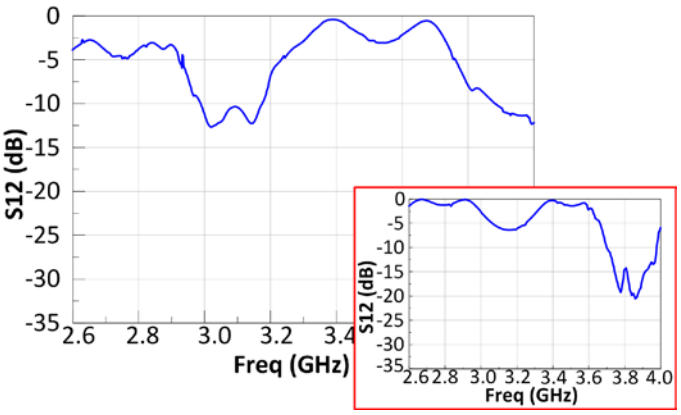

Fig. 7.12. Comparison of measured S12 for fluidic network and similar static test.

During injection of the 20% volume fraction mixture, the inlet and outlet layer separated and began to leak. This leakage is shown in Fig. 7.13. This caused the reservoirs to fill unevenly and no measurements were taken for this experiment.

Fig. 7.13. Damaged fluidic network.

A second fluidic network is completely reconstructed. However, the plasma bond fails again in the first test. New fabrication methods will be explored for future experiments. These will be discussed in Chapter VIII.

CHAPTER VIII

CONCLUSIONS

Summary

The four-arm spiral FSS demonstrated in this work provides TE and TM independence as well as operation over a wide angle of incidence away from broadside. These characteristics make the FSS functional for a variety of applications and antennas. Control over resonant frequency of the stop-band can be achieved by loading individual spirals of a four-arm spiral frequency selective surface with cylindrical dielectric dispersions. Size and composition of the dispersions are varied for tuning purposes. This provides a non-wired method of tuning. Non-wired tuning of the FSS provides the ability to reduce spurious radiation and reactive loading in use with antennas.

Static tests reveal the capability to control resonant frequency of the stop-band through varying the diameter of multiple types of dispersions: PDMS, Silicone Oil, and BSTO dispersed in PDMS and Silicone Oil at varying volume fractions. Two FSS sizes are used in the static tests: 3 by 7 and 8 by 8, with operating frequencies at 3.95 GHz and 3.91 GHz respectively. The desirable range of frequency control is across the S-band, 2.1 GHz – 4.0 GHz. Measurements present a similar tuning behavior as the simulations. However, the magnitude of frequency shift from experiments is not as great as the magnitude of shift from simulations. A maximum downward shift of .699 GHz is achieved with 5 mm Silicone Oil dispersions on the 3 by 7 array.

Simulations reveal that the lack of shift and loss of stop-band strength from measurements could be due to losses in the materials. Fabrication errors also contribute to loss of stop-band strength as well as multiple resonant frequencies. These errors can be minimized by improving placement of discs.

Multiple resonant frequencies can be achieved at once by loading a small group of spirals across the FSS. Static tests and the fluidic network revealed capability to open varying windows of stop-bands by altering the size and dielectric constant of the dispersions. Losses in the materials hindered the full tuning capability of the fluidic network FSS. Eliminating these losses can lead to greater control over range of tuning.

Future Work

The materials used in these experiments hindered the function of this design with their losses and low permittivities. Exploration of new materials for tuning can lead to improved tuning capability, i.e. magnetic materials, improved dispersion particle shapes.

New designs for fluidic networks are being considered. The designs eliminate the use of a PDMS dispersion layer. The use of Duroid as the dispersion layer and channel layers can eliminate some losses from PDMS and improve precision of aligning layers. A milling machine is used to mill the channels and dispersions in the Duroid. This method is very precise and speedy compared to PDMS fabrication. Another design option is the use of air channels to eliminate the need of flowing very thick mixtures through thin channels. The air channels will push dispersions above the spirals. This provides a possible opportunity to team up with MEMS students for materials and design knowledge.

REFERENCES

[1] N. Behdad, "A Low-Profile Third-Order Bandpass Frequency Selective Surface," *IEEE Trans. Microwave Theory Tech.*, vol. 56, pp. 774-781, 2008.

[2] F. Bayatpur and K. Sarabandi, "Single-Layer High-Order Miniaturized-Element Frequency Selective Surfaces," *IEEE Trans. Antennas Propag.*, vol. 57, pp. 460-466, 2009.

[3] K. Sarabandi and N.Behdad, "A Frequency Selective Surface With Miniaturized Elements," *IEEE Trans. Antennas Propag.*, vol. 55, pp. 1239-1245, 2007.

[4] N. Behdad, "Miniaturized-element Frequency Selective Surfaces (MEFSS) Using Sub-wavelength Periodic Structures," in *Radio and Wireless Symp.*, 2008, pp. 347-350.

[5] C. Mias, "Tunable C-Band Frequency Selective Surface," in *Proc. IEE Wideband and Multi-band Antennas and Arrays Conf* , 2005, pp. 165-169.

[6] F. Bayatpur and K. Sarabandi, "A tunable, band-pass, miniaturized-element frequency selective surface: Design and measurement," in *IEEE Antennas Propag. Internat. Symp.*, 2007, pp. 3964-3967.

[7] G.M.Coutts, R.R.Mansour, and S.K.Chauhuri, "A MEMS-Tunable Frequency-Selective Surface Monolithically Integrated on a Flexible Substrate," in *IEEE/MMT-S Internat. Microwave Symp.*, 2007, pp. 497-500.

[8] G.H.Huff and S. Goldberger, "A Coaxial Stub Microfluidic Impedance Transformer (COSMIX)," *IEEE Microwave and Wireless Components Letters*, vol. 20, pp. 154-156, 2010.

[9] S.A.Long and G.H.Huff, "A Substrate Integrated Fuidic Compensation Mechanism for Deformable Antennas," *AHS NASA/ESA Conf. Adaptive Hardware and Systems*, 2009, pp. 247-251.

[10] C.D.Karp, "Microfluidic filter," U.S. Patent 6811695, Nov. 02, 2004.

[11] Getting Started with HFSS: Floquet Ports, Ansoft Corp., Pittsburgh, PA, July 2007. Available www.eecis.udel.edu/~spencer/HFSSFloquet.pdf

VITA

Name:	Elizabeth Christine Wells
Address:	Department of Electrical Engineering, Texas A&M University, College Station, TX 77843
Email Address:	teamhames724@gmail.com
Education:	B.S., Electrical Engineering, Texas A&M University, 2009 M.S., Electrical Engineering, Texas A&M University, 2011